

A natural example of the disequilibrium breakdown of biotite at high temperature: TEM observations and comparison with experimental kinetic data

A. J. BREARLEY*

Department of Geology, The University, Manchester M13 9PL

Abstract

Transmission electron microscopy has been used to investigate the mechanism of natural biotite breakdown under pyrometamorphic disequilibrium conditions. Biotite in a xenolith of pelitic gneiss collected from a Tertiary dolerite sill, Isle of Mull, Scotland, shows evidence of an incipient reaction, characterised by a darkening in colour and the appearance of areas of fine-grained reaction products. TEM and analytical electron microscope data show that the reaction can be described as:

Fe-Al biotite \rightarrow Mg-Al biotite + magnetite + hercynitic spinel + K-feldspar/melt + vapour.

The orientations of the product phase are controlled by the crystallography of the reacting biotite, demonstrating that the transformation proceeds by a topotactic mechanism. An empirical method, based on the Mg/(Fe²⁺ + Fe³⁺) ratios of coexisting spinel and biotite from experimental data, is used to deduce that the reaction occurred above ~ 770 °C. A comparison of the natural reaction microstructures with those produced experimentally suggest that the xenolith was probably above 800 °C for less than 48 hours and cooled to temperatures of 770 °C after ~ 150 –200 hours.

KEYWORDS: transmission electron microscopy, biotite, pyrometamorphism.

Introduction

MANY metamorphic reactions which occur under disequilibrium conditions in, for example, contact aureoles of igneous intrusions, exhibit evidence of only partial mineral transformation. This is especially true of reactions which take place during pyrometamorphism and involve the breakdown of relatively coarse-grained phases. The entire sequence of heating and cooling events is highly compressed and preservation of stranded reaction microstructures is favoured. Recent electron microscope studies of the breakdown of micas in nature (e.g. Brearley, 1984, 1986, on phengite; Worden *et al.* (this vol.) on phengite and chlorite) and experimentally (e.g. Rubie and Brearley, 1986, 1987, on muscovite; Brearley, 1987, on biotite) show that the reaction products are fine-grained and intimately intergrown with the precursor phase. It has been possible in each case to elucidate a detailed reaction mechanism for the transformation. The present study reports a further example of such

* Present address: Institute of Meteoritics, Dept. of Geology, University of New Mexico, Albuquerque, New Mexico 87131, USA.

a reaction; that of the incipient breakdown of biotite in a xenolith of pelitic gneiss during pyrometamorphism.

Several examples of advanced biotite breakdown under similar metamorphic conditions, some involving a melting reaction, have been reported (e.g. Le Maitre, 1974; Grapes, 1986; and Pichavant, pers. comm.). The reaction is therefore of some interest to petrologists, because the extent of transformation observed in xenoliths can reveal important information on the cooling rates of the intrusion which contains them. In this paper I attempt to constrain possible reaction times, and hence cooling rates, using observed natural mineral reaction microstructures and comparing them with available experimental kinetic data.

Sample locality

The sample studied is a xenolith of pelitic gneiss collected from a dolerite sill on the Ross of Mull, Isle of Mull, Scotland. The sill is part of the Loch Scridain suite of Tertiary intrusions which outcrop on the southwestern part of Mull. The sill in question is approximately 2 m thick and was

intruded into a sequence of interbedded pelitic, psammitic and calcareous metasediments of the Moine series (Brearley, 1986). Numerous xenoliths of all these lithologies, ranging from a few centimetres up to one metre in diameter, occur throughout the sill. This study is restricted to a sample taken from the rim of a pelitic xenolith (30 cm in diameter) collected from the upper surface of the sill.

Petrography

The detailed petrography and mineral chemistry of this rock have been reported by Brearley (1986). The xenolith is a coarse-grained, pelitic gneiss with a strong metamorphic foliation and contains the optically observable mineral assemblage: garnet + biotite + muscovite + plagioclase + ilmenite. Quartz is, surprisingly, absent. The muscovite is almost completely pseudomorphed by an extremely fine-grained intergrowth of phases which has been investigated in detail by Brearley (1986). The co-existing biotite does not appear to have reacted as extensively as the muscovite. It exhibits a marked darkening in colour in the core regions (Fig. 1) but the rims are apparently unaffected and are a much lighter brown. In addition, evidence of the development of very fine-grained reaction products locally within the biotite is detectable by high-magnification light microscopy.

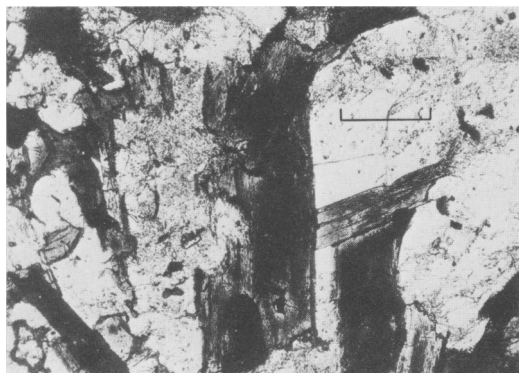


FIG. 1. Optical micrograph (plane polarised light) of partially transformed biotite crystals from xenolith, exhibiting marked darkening in the core region. Scale bar = 0.3 mm.

Electron probe microanalysis

The chemistry of the biotites has been investigated extensively by electron microprobe to establish whether the optically observed variations between rim and core are due simply to compositional variations. The analytical data show that,

in every case, the biotites are chemically homogeneous except for very slight increases (1–2 wt. %) in SiO_2 and MgO and a decrease in TiO_2 at the very edge of the biotite. No variations have been observed which can explain the optical properties.

Compositionally the biotites tend towards siderophyllite with around 2.4–2.5 Al cations in tetrahedral co-ordination and $\text{Mg}/(\text{Mg} + \text{Fe})$ ratios of between 0.36 and 0.4. Representative electron microprobe analyses are reported in Table 1.

Table 1: Electron microprobe analyses of biotite from xenolith

SiO_2	35.18	35.92	35.07	35.05	35.76
TiO_2	3.04	2.44	2.89	3.37	3.35
Al_2O_3	17.05	17.28	17.52	17.51	17.44
FeO	22.96	22.65	22.85	22.56	22.48
MnO	—	0.20	0.20	0.34	0.24
MgO	7.46	7.78	7.22	7.62	7.51
CaO	—	—	—	—	—
Na_2O	0.44	—	—	0.42	0.46
K_2O	8.98	8.69	8.65	9.05	9.12
BaO	0.46	—	—	—	—
Total	95.57	94.96	94.44	95.92	96.36
Formulae recalculated on the basis of 22 [O] atoms					
Si	5.460	5.553	5.471	5.397	5.468
Ti	0.355	0.284	0.339	0.391	0.385
Al	3.118	3.148	3.222	3.178	3.144
Fe	2.979	2.928	2.981	2.905	2.876
Mn	—	0.027	0.027	0.045	0.032
Mg	1.730	1.794	1.698	1.748	1.712
Ca	—	—	—	—	—
Na	0.133	—	—	0.124	0.135
K	1.778	1.713	1.721	1.778	1.779
Ba	0.028	—	—	—	—
$\text{Mg}/(\text{Mg} + \text{Fe})$	0.360	0.379	0.362	0.375	0.373

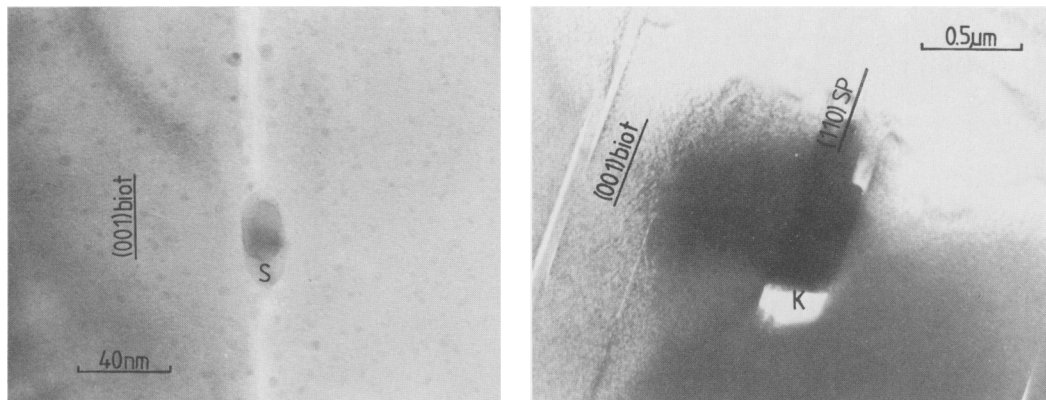
Transmission electron microscopy: experimental methods

Crystals of biotite were selected from doubly-polished, petrographic thin-sections and were ion-thinned using ion-beam bombardment techniques (Barber, 1970). The transmission electron microscopy (TEM) was performed on a Philips EM 400T operating at 100 kV throughout, using a double-tilt goniometer stage fitted with a beryllium insert to minimise extraneous X-ray production. *In-situ* X-ray microanalysis was carried out using an EDAX 9100 EDS spectrometer.

Transmission electron microscopy: observations

The lighter rim regions ($\sim 40 \mu\text{m}$ inward from the edge of the biotite) were initially investigated in the TEM. It was found that the rims of the biotite exhibited no evidence of any reaction microstructure. No second phases except inclusions of ilmenite were found.

However, on moving to the darker core region of the biotite evidence of a transformation was observed. Occasional particles of a second phase,



Figs. 2 and 3. Fig. 2 (*left*). Transmission electron micrograph showing a small magnetite-rich particle (S) which has nucleated on and grown parallel to a prominent (001) cleavage plane in biotite. Fig. 3 (*right*). Electron micrograph of hercynite-rich spinel (S) within ordered biotite. An associated volume of K-feldspar (K) is indicated.

around 200 Å in diameter and 400–500 Å in length, have nucleated along prominent (001) cleavage planes in the biotite (Fig. 2). Using a combination of X-ray microanalysis and microdiffraction techniques (Brearley and Champness, 1986) these particles were identified as magnetite. As well as the particles of magnetite a much larger spinel phase was also found. These spinels have nucleated both within ordered biotite (Fig. 3) and along prominent cleavage planes and may be up to 0.75 μm in length. Analytical data (see below) show that these large spinels may be either magnetite or pleonaste compositionally very distinct from the magnetite. The latter are by far the most abundant. It seems probable that the combination of development of the particles of magnetite and the larger spinels is responsible for the darkening in colour of the biotite observed by optical microscopy.

As in all the cases of mica breakdown studied by TEM in either natural or experimentally reacted samples (e.g. Brearley, 1986; Rubie and Brearley, 1986), the orientations of the reaction products are invariably controlled by the layer structure of the mica. The breakdown of biotite is no exception, and the spinel is strongly oriented relative to the biotite with the crystallographic relationship: $(001)_{\text{biot}} \parallel \{110\}_{\text{sp}} \cdot [010]_{\text{biot}} \parallel \langle 111 \rangle_{\text{sp}}$. It is of interest that the expected orientation relationship between the two phases, with the planes of close-packed oxygen atoms parallel, i.e. $(001)_{\text{biot}} \parallel (111)_{\text{sp}} \cdot [010]_{\text{biot}} \parallel [110]_{\text{sp}}$, has not been observed. This orientation relationship is, however, commonly found in experimentally reacted biotites (Brearley, 1987).

In addition to the development of the spinel

phase, areas of alkali feldspar have formed in elongate volumes parallel to the basal plane of the biotite (Fig. 4a) and may or may not be associated with the development of spinel. In the earliest stages of formation, the regions of alkali feldspar may only be 0.1 μm in width, but where more extensive reaction has taken place larger areas (0.5–0.9 μm in width) have formed. The morphology of the product K-feldspar, i.e., elongate parallel to $(001)_{\text{biotite}}$, suggests that there is a crystallographic relationship between the two phases. Electron diffraction studies show that this orientation relationship is $(001)_{\text{biot}} \parallel (010)_{\text{Kfs}} \cdot [010]_{\text{biot}} \parallel [102]_{\text{Kfs}}$.

As well as areas of alkali feldspar, small lenses of a glass phase have been found within the biotite (Fig. 4b). These also have an elongate morphology parallel to $(001)_{\text{biotite}}$ and may be up to 0.05 μm in width.

At more extensive degrees of reaction, quite large volumes of alkali feldspar develop within the biotite. When examined with the electron beam parallel to the *c*-axis of the mica, the biotite is found to have a curved interface with the alkali feldspar comparable with that observed by Brearley (1986) in reacted phengites. In contrast the interface between these two phases along $(001)_{\text{biotite}}$ is always planar as shown in Fig. 4a.

Although the outer, light-coloured areas of the biotite show no evidence of reaction, a narrow region (~4 μm wide) at the grain boundary with muscovite or plagioclase is often found to be extensively transformed. In these areas abundant spinel and alkali feldspar coexist (Fig. 5) and the advanced progress of the reaction suggests that reaction rates were enhanced by nucleation at

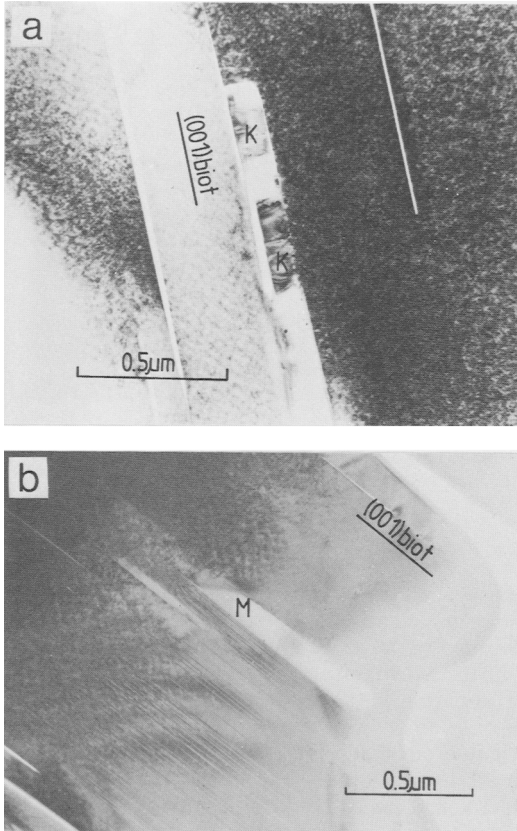


FIG. 4. (a) An isolated, elongate volume of alkali feldspar (K) within biotite which has grown parallel to the basal, (001) mica plane. (b) Transmission electron micrograph of elongate volume of melt (M) which has developed within biotite.

a grain boundary. The catalytic effects of fluid released from the dehydration of adjacent phengite probably also played an important role in locally increasing the reaction rate (Rubie, 1986).

Analytical electron microscopy

The mineral chemistries of the coexisting phases involved in the reaction have been studied in detail by analytical electron microscopy, using the thin film approximation of Cliff and Lorimer (1975). This method necessitates the normalisation of all the data to 100%, as reported in Tables 2 and 3.

Spinel

The analytical data for the spinels fall into two distinct groups, one being almost pure magnetite and the other a hercynite-rich spinel. The only

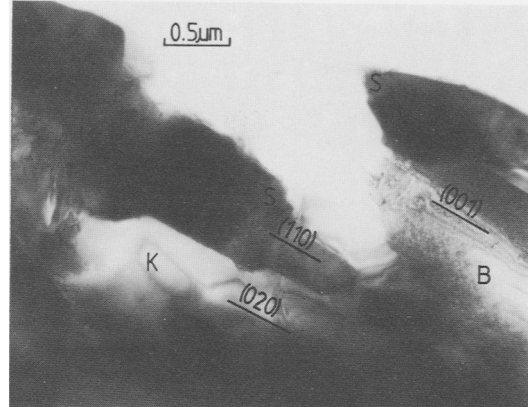


FIG. 5. Region of extensively transformed biotite adjacent to a grain boundary with muscovite consisting of an intergrowth of oriented spinel (S), new biotite (B) and K-feldspar (K).

exceptions to this are spinels adjacent to the grain boundary which have compositions around magnetite₄₀hercynite₆₀. The rest of the spinel compositions can be adequately described in terms of the three end-members hercynite-magnetite-spinel but ulvöspinel ($\text{Fe}_2\text{TiO}_4 = 1-2\%$), galaxite ($\text{MnAl}_2\text{O}_4 = 1-2\%$) and gahnite ($\text{ZnAl}_2\text{O}_4 = 1-6\%$) are also minor components in the spinel. Representative analytical data are reported in Table 2. The spinel formulae have been calculated assuming 32[O] and 24 cations per formula unit. Analytical data in terms of the three most abundant end-members are shown in Fig. 6 together with the compositions of spinels in the coexisting phengite pseudomorphs (from Brearley, 1986). Some other spinel compositions reported in the literature by Abraham and Schreyer (1973), Smith (1965), Stewart (1942), Grapes (1986) and the experimental data of Brearley (1987) for spinels in biotite reacted at 800 °C and 850 °C (Brearley, unpublished data) are shown for comparison. The magnetite contents of the spinels from the biotite in this study range between 2 and 25% and they are considerably more iron-rich than the spinels from the muscovite pseudomorphs studied by Brearley (1986). The former are comparable in composition with spinels which developed in reacted biotites studied by Grapes (1986).

Biotite

The changes in biotite chemistry which accompany the development of spinel and K-feldspar have been investigated in detail by AEM. Representative analyses of biotite coexisting with alkali

Table 2: Analytical electron microscope analyses of spinels from reacted biotite

	1	2	3	4	5	6
SiO ₂	-	-	-	-	-	-
TiO ₂	0.81	0.41	0.41	0.22	1.91	1.38
Al ₂ O ₃	54.82	52.99	49.04	46.12	39.59	33.05
Fe ₂ O ₃	6.16	8.39	12.16	15.35	18.63	27.02
FeO	30.74	33.07	34.39	31.24	32.62	32.54
MnO	0.34	0.42	0.56	0.44	0.63	0.59
MgO	6.10	4.72	3.36	2.49	0.71	-
ZnO	1.03	na	na	4.14	5.91	5.42
Total	100.00	100.00	100.00	100.00	100.00	100.00

Formulae recalculated on the basis of Σ cations = 24.000 and 32 [O]

Si	-	-	-	-	-	-
Ti	0.137	0.071	0.088	0.039	0.362	0.271
Al	14.673	14.400	13.660	13.132	11.746	10.158
Fe ³⁺	1.052	1.456	2.160	2.789	3.259	5.300
Fe ²⁺	5.838	6.373	6.794	6.312	6.865	7.095
Mn	0.067	0.081	0.113	0.091	0.134	0.131
Mg	2.058	1.618	1.181	0.897	0.265	-
Zn	0.175	-	-	0.739	1.098	1.045

Endmembers

SP	25.72	20.23	14.76	11.21	-	3.31
HER	62.96	68.75	69.21	60.49	48.79	54.70
MAG	6.57	9.09	13.52	17.43	33.13	22.06
GAL	0.84	1.02	1.41	1.13	1.64	1.67
GAH	2.19	-	-	9.24	13.06	13.72
ULV	1.72	0.90	1.09	0.49	3.38	4.53

SP = MgAl₂O₄ (spinel); HER = FeAl₂O₄ (hercynite); MAG = Fe₃O₄ (magnetite); GAL = MnAl₂O₄ (galaxite); GAH = ZnAl₂O₄ (gahnite); ULV = Fe₂TiO₄ (ulvöspinel)

Analyses 1-4: Spinel from core region of biotite coexisting with K-feldspar.

Analyses 5-6: Spinel adjacent to grain boundary with muscovite in highly transformed biotite.

feldspar (or glass) and spinel are reported in Table 3 with formulae recalculated on the basis of 22[O] atoms.

The AEM investigations suggest that stranded diffusion profiles are present in biotite immediately adjacent to spinel and K-feldspar. Biotite within

0.5 μm of the spinel-biotite interface has a higher Mg/Fe ratio than biotite 5 μm or more from the spinel. Because of the presence of such diffusion profiles in the biotite it is necessary to analyse as close to the spinel as possible (within 100 nm of the interface) in order to obtain the true composition of the biotite. However, experimental requirements (such as tilting) may not always be compatible with this requisite and it is inevitable that, in some cases, analyses of biotite slightly further away from the spinel with different Mg/Fe ratios will be obtained.

The most important compositional changes in the biotite which result from the development of spinel and K-feldspar are summarised in Fig. 7a and b. Bulk electron microprobe analyses of biotites have Mg/Fe ratios of 0.5-0.7 and Al contents of > 3.1 (Fig. 7a). In comparison, the AEM data show that biotite immediately adjacent to spinel and K-feldspar becomes progressively more Mg-rich and less aluminous as the reaction proceeds. The increase in Mg is extremely marked; some of the biotites coexisting with spinel have Mg/Fe ratios up to 0.9 and Al contents of 2.9.

Coupled with the decrease in Al is an increase in the Si content of the remaining biotite (Fig. 7b). With increasing reaction there is a significant, and almost linear increase in Si which is coupled with a decrease in Al content. This is the same

Table 3: Analytical electron microscope analyses of biotites* adjacent to areas of spinel and alkali feldspar development

SiO ₂	39.29	40.71	40.97	38.98	39.63
TiO ₂	3.23	4.99	2.80	3.27	1.91
Al ₂ O ₃	16.33	17.61	17.39	17.83	18.70
FeO ^a	24.35	18.50	20.43	22.42	21.75
MnO	0.26	-	-	0.23	0.19
MgO	5.74	9.25	9.22	8.59	8.86
ZnO	0.82	-	na	na	na
CaO	-	-	-	-	-
Na ₂ O	-	-	-	-	-
K ₂ O	8.94	9.98	9.19	8.68	9.14
Total	100.00	100.00	100.00	100.00	100.00

Recalculated formulae based on 22[O] atoms

Si	5.824	5.777	5.868	5.683	5.716
Ti	0.360	0.533	0.302	0.357	0.208
Al	2.854	2.946	2.937	3.049	3.178
Fe	2.914	2.196	2.447	2.720	2.623
Mn	0.012	-	-	0.028	0.023
Mg	1.268	1.956	1.968	1.857	1.914
Ca	-	-	-	-	-
Na	-	-	-	-	-
K	1.687	1.617	1.679	1.604	1.682
Mg/(Mg+Fe)	0.303	0.471	0.445	0.405	0.420

* Normalised to 100%

^a Total Fe calculated as Fe²⁺

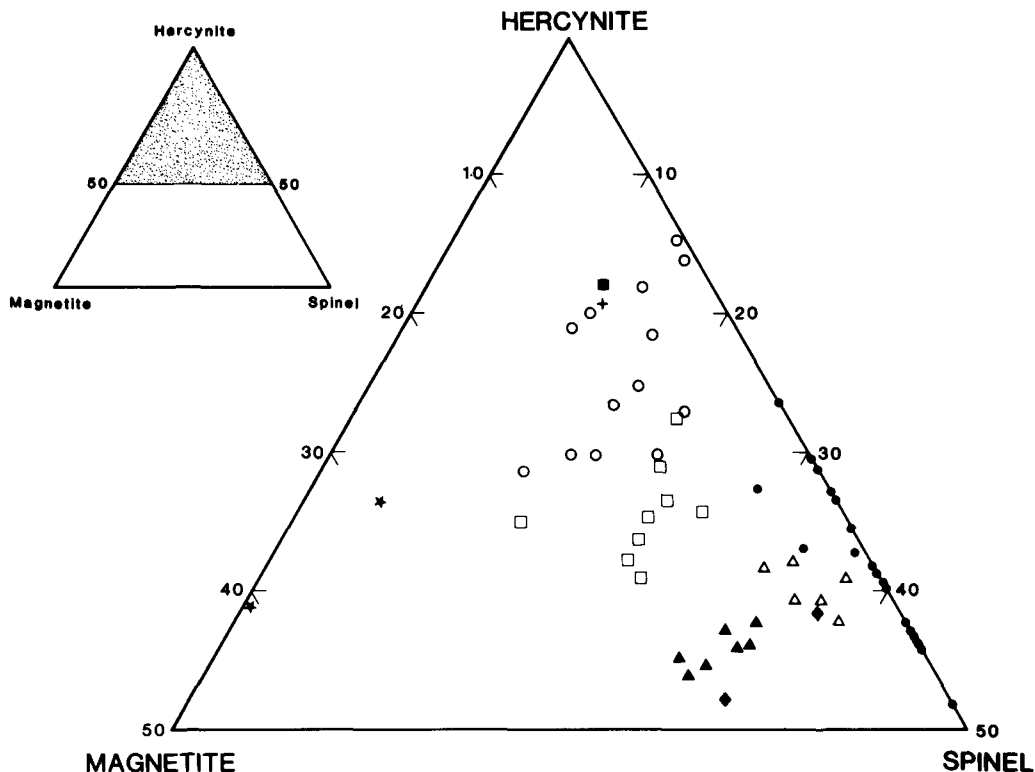


FIG. 6. Compositions of analysed pleonaste spinels from this study and those reported in the literature in terms of the end-members hercynite (FeAl_2O_4), spinel (MgAl_2O_4) and magnetite (Fe_3O_4). Open circles = spinels from reacted biotite (this study), stars = spinels on rim of biotite coexisting with K-feldspar (this study), closed circles = spinels from coexisting muscovite pseudomorph (Brearley, 1986), open squares = spinels from experimentally reacted biotite (800 °C, 1 kbar, QFM buffer, Brearley, 1987), open triangles = spinels from experimentally reacted biotite (850 °C, QFM buffer, Brearley, unpublished data). *Other data*: closed triangles = spinels from reacted biotite (Grapes, 1986) compositionally comparable to biotite used for experimental study of Brearley (1987), closed squares = spinels from iron-rich hornfels (Abraham and Schreyer, 1973), crosses = spinel from Al-rich hornfels (Stewart, 1942), closed diamonds = least oxidised spinels of Smith (1965) from contact emery rocks.

compositional trend observed by Brearley (1987) in experimentally reacted biotites, but is inconsistent with the phase equilibrium data of Rutherford (1973) who found that biotites became more aluminous.

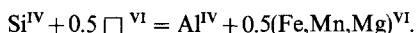
A more detailed analysis of the compositional variations observed in the reacting biotite have been carried out using the data obtained by AEM and the results are summarised in Fig. 8a-d. These data reveal the following substitutional relationships:

- (i) The octahedral site occupancy decreases with increasing Si, i.e. the number of vacancies increases (Fig. 8a);
- (ii) $\Sigma\text{Fe} + \text{Mn} + \text{Mg}$ decreases with increasing Si, i.e. as the reaction proceeds (Fig. 8b);
- (iii) Ti increases as Al^{VI} decreases, but this

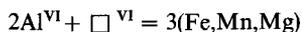
substitution shows no clear relationship with the degree of reaction (Fig. 8c);

- (iv) $\Sigma\text{Al}^{\text{VI}} + \text{Ti}$ increases as $\Sigma\text{Fe} + \text{Mn} + \text{Mg}$ decreases (Fig. 8d).

These data suggest that there are three main substitutions which control the biotite chemistry during the reaction. The correlations of Si with both $\Sigma\text{Fe} + \text{Mn} + \text{Mg}$ and octahedral site occupancy suggest a relationship such as:



This substitution increases the number of vacancies in the octahedral sites. In addition, the inter-relationship between $\Sigma\text{Al}^{\text{VI}} + \text{Ti}$ and $\Sigma\text{Fe} + \text{Mn} + \text{Mg}$ indicates that there is a second substitution on the octahedral sites such as:



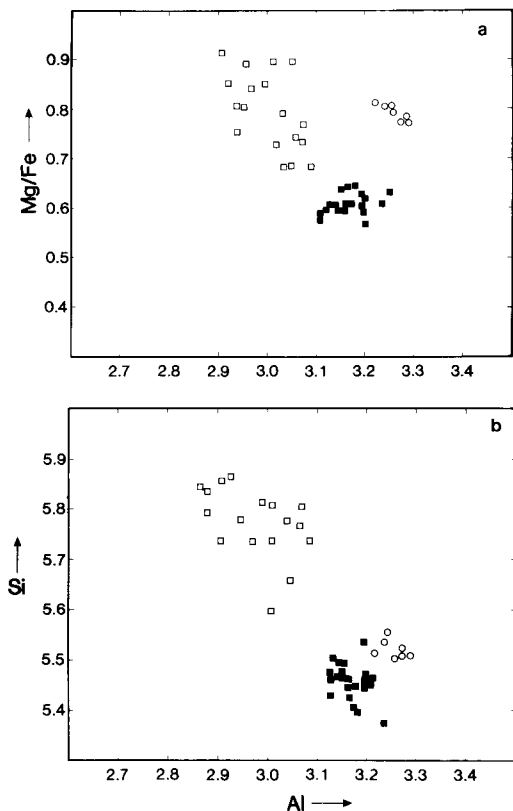


FIG. 7. (a) Plot of biotite Mg/Fe ratios vs. Al (cations based on 22[O] atoms). (b) Plot of biotites Si vs. Al (cation based on 22[O] atoms). Full squares = bulk electron microprobe analyses of biotite. Open squares = analytical electron microscope analyses of biotite immediately adjacent to spinel and alkali feldspar. Open circles = electron microprobe analyses of biotites from experimental study of Brearley (1987).

which operates simultaneously with a substitution between Al^{VI} and Ti of the type:



It is interesting that no Tschermak-type substitutions, $(MgFe)Si = Al^{VI}Al^{IV}$, operate during the reaction.

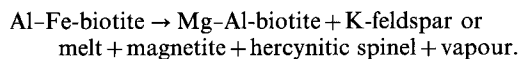
In summary, the progressive reaction of the biotite involves increased substitution of Si into the tetrahedral sheet of the mica and a decrease in ΣAl . The increase in Si is correlated with a decrease in $\Sigma Fe + Mn + Mg$ and an increase in the number of octahedral vacancies. Coupled with the decrease in total Al there is a significant increase in the Mg/Fe ratio of the biotite with increasing reaction.

Alkali feldspar

Some of the problems of analysing alkali feldspar in the transmission electron microscope have been discussed elsewhere (McGill and Hubbard, 1981) and will not be addressed here. Using the techniques outlined in Brearley (1986) it has been possible to ascertain that the feldspar produced in the reaction has a range of compositions between $Or_{95}Ab_5$ and $Or_{85}Ab_{15}$.

Discussion

The electron optical and analytical studies show conclusively that the breakdown of biotite can be described schematically by the reaction:



This reaction in the end-member iron system has been investigated by Rutherford (1973) who determined the equilibrium breakdown curves for Al-Fe biotite under varying conditions of f_{O_2} . This work was an extension of the classic experimental studies of Eugster and Wones (1962) on annite and Wones and Eugster (1965) on annite-phlogopite solid solutions. Rutherford showed that an aluminous iron biotite, heated along a given oxygen buffer curve, decomposed progressively to a new, more aluminous biotite, plus hercynite, magnetite, K-feldspar, leucite and vapour. The experimental work on the effect of Mg on the stability of biotite, although only investigated for biotites along the annite-phlogopite join, suggests that aluminous Mg-Fe biotites should also become more Mg-rich with increasing temperature. The analytical data from this study clearly demonstrate this to be the case, but also show that the biotites become more siliceous (Fig. 7b), rather than more aluminous, during the reaction. This is clearly inconsistent with the experimental work of Rutherford (1973) and suggests that the effect of Mg on the phase relations in the aluminous system is considerable.

The compositional relations of the coexisting minerals in the reaction are summarised in Fig. 9, a ternary $Al_2O_3-FeO-MgO$ mole percent diagram. All the phases coexist with K-feldspar or glass. The bulk electron microprobe analyses of the biotites are plotted and lie within the three-phase triangle defined by the compositions of coexisting spinel, magnetite and remaining biotite. The biotite becomes more Mg-rich during the reaction but on this diagram the trend towards Al-poor compositions away from the bulk biotite compositions is not clear. This is probably due to the decrease in $\Sigma Mg + Fe$ in the octahedral sites (Fig. 8b) so that the ratio $Al/(Mg + Fe)$ only decreases slightly during the reaction.

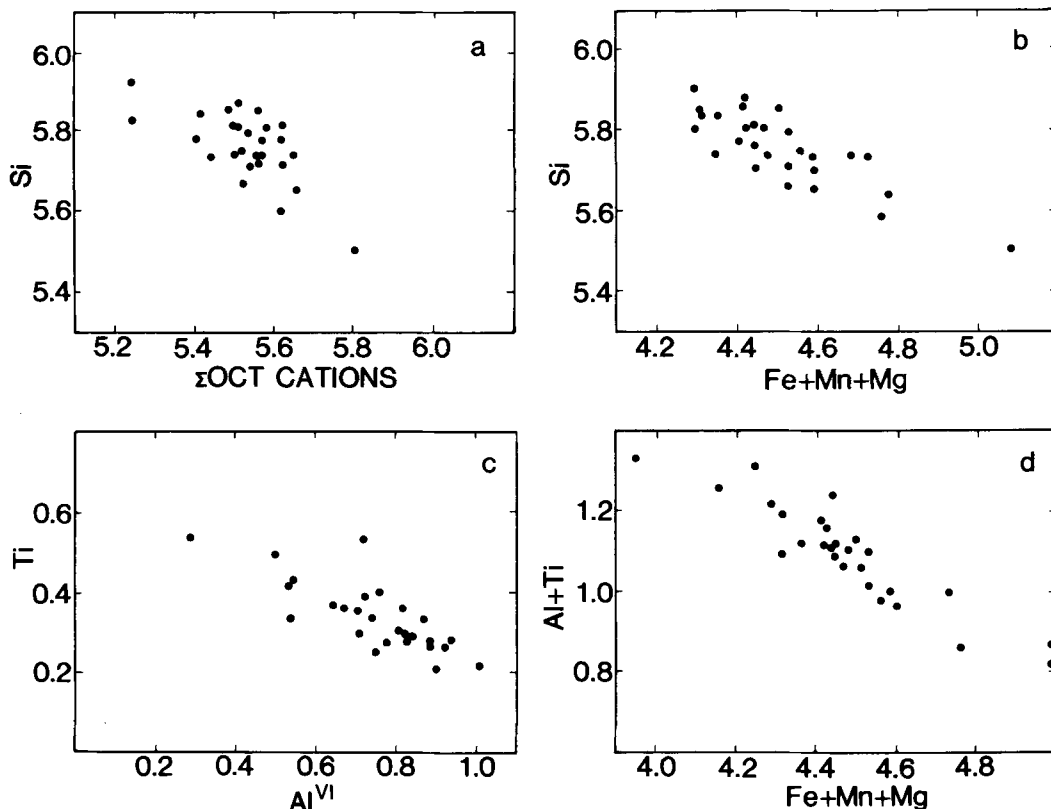
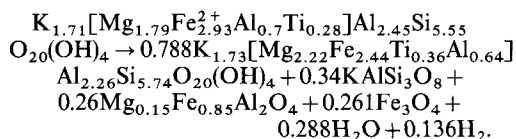


FIG. 8. Bivariate plots showing substitutional relationships in biotite coexisting with spinel and K-feldspar (analytical electron microscope analyses). (a) Si vs. Σ octahedral cations; (b) Si vs. Σ Fe + Mn + Mg; (c) Ti vs. octahedral Al; (d) Octahedral Al + Ti vs. Σ Fe + Mn + Mg. Cations based on 22[O] atoms.

A balanced reaction can be calculated for the transformation using the analysed mineral compositions for the coexisting phases. It has been assumed that the reaction is essentially isochemical with the exception of hydrogen. The Fe^{3+} content of the precursor biotite is unknown, but according to Wones *et al.* (1971) is usually low (< 10% of the total iron) under conditions of the QFM buffer. For the purposes of this study it has been assumed that the Fe^{3+} content is zero in both reactant and product biotites (see also Labotka, 1983). Any Fe^{3+} which may be present will be involved in producing magnetite, but it is most probable that oxidation of Fe^{2+} to Fe^{3+} takes place during the reaction due to loss of hydrogen. Balancing of the reaction has been carried out by the solution of a set of linear equations to determine the reaction coefficients for each phase in the reaction, e.g. Spear *et al.* (1982). In this case, because the number of phases is less than the number of components necessary to describe

the phases, the solution is not exact. Exact balance of the reaction has been achieved by adjusting the alkali site occupancies of the reactant and product biotites. The resultant possible balanced reaction using simplified mineral formulae is given below



One problem with the reaction scheme concerns the change in the Ti content of the biotite as the reaction progresses. Theoretically the Ti content of the remaining biotite should increase because no discrete Ti-bearing phases are produced in the reaction. However, this is not obvious from a comparison of the electron microprobe data and the AEM data from biotite adjacent to spinel (Tables 1 and 3). This suggests that there may be a

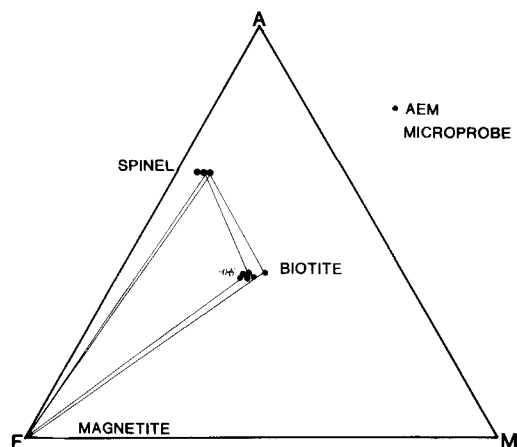


FIG. 9. Ternary Al_2O_3 - FeO - MgO mole percent diagram showing compositions of coexisting phases in the reacting biotites. Open squares = bulk electron microprobe analyses of biotite; closed circles = analytical electron microscope analyses from biotite and spinel coexisting with K-feldspar.

discrepancy (~ 0.5 wt. % TiO_2) between the two techniques (microprobe and AEM) due to slight calibration differences, which would be sufficient to obscure the predicted increase. A further contributing factor which might obscure the increase is the variation in the Ti content of the biotite as shown by the electron microprobe analyses (Table 3).

Reaction progress and comparison with experimental kinetic data

The kinetics and mechanisms of biotite breakdown under disequilibrium conditions have recently been investigated experimentally by Brearley (1987) using natural biotite within a rock matrix. The composition of the biotite used in the experiments is similar to that of the biotite reported in this study and this enables a reasonable comparison to be made between the two examples. Some typical biotite compositions have been plotted in Fig. 7a and b. In detail the biotite used for the experiments are more Mg-rich, with Mg/Fe ratios between 0.72 and 0.81 (c.f. 0.58-0.62) and are also rather more aluminous (3.2-3.3 Al per 22[O], c.f. 3.1-3.5).

Both rocks were collected from the Ross of Mull, Isle of Mull, Scotland, and the pre-contact metamorphic history of the xenolith reported here can be considered to have been identical to that of the sample used in the experiments. Both rocks were originally regionally metamorphosed at PT conditions of about 7 kbar, 550 ± 25 °C calculated from calibrated geothermometers and geobarometers

(Brearley, 1984). The effect of the incorporation of the xenolith into the sill is thus to overstep the original temperature of crystallisation by about 250 °C (see later), a considerable departure from equilibrium.

Experimental conditions were selected to approach as closely as possible the P - T conditions experienced by the xenolith. Runs have been carried out at 800 °C (Brearley, 1987) and 850 °C (Brearley unpublished data) using a QFM buffer assemblage to control f_{O_2} . From a consideration of the possible intrusion temperature of the magma and the cooling history (Brearley, 1986), this range of temperatures is reasonable. The exact pressure at which the sill was originally intruded cannot be estimated accurately, but between 0.5 and 1 kbar is likely to be a good estimate. The experiments were therefore all performed at a pressure of 1 kbar. The effect of pressure on the position of the equilibrium breakdown curve (and hence the estimated degree of reaction overstepping) is likely to be of relative importance in dehydration reactions of this kind because of the curvature of the reaction boundary towards the pressure axis with increasing temperature. In the case of biotite the experimental data of Eugster and Wones (1962) for the dehydration of the iron end-member, annite, show that the reaction at 1 kbar proceeds at a temperature 40 °C higher than at 0.5 kbar. However, in the case discussed here, where the overstepping temperature ΔT is around 250 °C, this may not have a very significant effect. Nevertheless the effect of pressure is currently under investigation.

The experimental data enable information of two types to be extracted from the natural example. Firstly the approximate temperature at which the reaction occurred can be estimated on an empirical basis from the experimental data, and secondly a semi-quantitative estimate of the period of time over which the reaction occurred can also be made from (a) a comparison of the reaction microstructures and (b) the mineral chemistry.

Temperature estimates

An analysis of the compositions of coexisting spinel and biotite from the experimental runs has shown that the ratio $\text{Mg}/(\text{Fe}^{2+} + \text{Fe}^{3+})_{\text{biotite}} : \text{Mg}/(\text{Fe}^{2+} + \text{Fe}^{3+})_{\text{spinel}}$ can be used as an empirical indicator of temperature despite the lack of equilibrium in the experiments. This is illustrated in Fig. 10, a plot of $\text{Mg}/(\text{Fe}^{2+} + \text{Fe}^{3+})_{\text{biotite}}$ against $\text{Mg}/(\text{Fe}^{2+} + \text{Fe}^{3+})_{\text{spinel}}$ for coexisting biotite and spinel from experimental runs at 800 and 850 °C. The lines of best fit for the data at each of the two temperatures are shown and demonstrate that with increasing T the spinel produced in the reaction

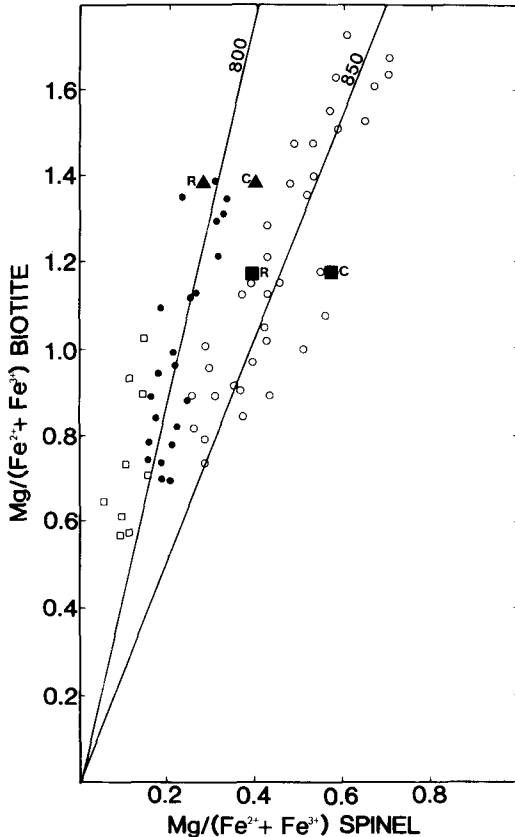


FIG. 10. Diagram showing relationship between the $\text{Mg}/(\text{Fe}^{2+} + \text{Fe}^{3+})$ ratios of coexisting biotite and spinel as a function of temperature in disequilibrium experiments at 1 kbar (QFM oxygen buffer). Lines of best fit for 800 and 850 °C are shown from the data of Brearley (1987) for 800 °C (closed circles) and Brearley (unpublished data) for 850 °C (open circles). Open squares are data from naturally-occurring coexisting spinel and biotite in this study. Closed squares: spinel rim (R) and core (C) compositions coexisting with partially melted biotite from Grapes (1986); closed triangles: spinel rim (R) and core (C) compositions coexisting with new biotite also from Grapes (1986).

becomes progressively more Mg-rich. Biotite compositions were obtained from within 100 nm of the spinel using a 50 nm electron beam diameter. Some of the spread in the data can be accounted for by the large compositional gradients in Mg and Fe in the biotite adjacent to the spinel as discussed earlier.

It should be noted that the data are from experiments of run durations between 24 and 1600 hours in which equilibrium was not attained. It is found that the compositions of the spinels and adjacent biotite change as a function of time, both

phases becoming more Mg-rich ($\text{Mg}/\text{Fe}_{\text{spinel}} < \text{Mg}/\text{Fe}_{\text{reacting biotite}} < \text{Mg}/\text{Fe}_{\text{product biotite}}$). However, it is clear from Fig. 10 that, despite this compositional change, the ratio $\text{Mg}/(\text{Fe}^{2+} + \text{Fe}^{3+})_{\text{biotite}} : \text{Mg}/(\text{Fe}^{2+} + \text{Fe}^{3+})_{\text{spinel}}$ remains constant, so that with increasing run time the coexisting biotite and spinel evolve along a line of constant slope (see later). In equilibrium experiments this would be a line along which the partition coefficient (K_D) is constant, but the use of K_D is misleading in this context, because the two phases are clearly not in thermodynamic equilibrium.

The data for coexisting spinel and biotite from the natural example in this study are also plotted in Fig. 10. There is a systematic linear increase in the $\text{Mg}/\text{Fe}^{2+} + \text{Fe}^{3+}$ ratios of both phases, but at lower spinel $\text{Mg}/(\text{Fe}^{2+} + \text{Fe}^{3+})$ ratios than the experimental data for 800 °C. This clearly suggests that the spinels grew at temperatures around 770 °C (assuming the effects of pressure and the compositional differences between the biotites are negligible). This is a reasonable result from other considerations (see later), but a further test of the reliability of temperature estimates based on such an empirical method can be carried out using additional data from the literature. Grapes (1986) has recently reported electron microprobe data for spinels which have grown within reacted biotite from pelitic xenoliths. Grapes' electron microprobe data from (a) spinel coexisting with new or unmelted biotite and (b) spinel coexisting with partially melted biotite are plotted in Fig. 10. The composition of the precursor biotite was only slightly more Mg-rich than that used in the experiments of Brearley (1987) so direct comparison can be made with reasonable confidence. From other petrographic data Grapes suggested a temperature of at least 830 °C at pressures of 2–3 kbar for the xenolith containing the reacting biotite. The data for coexisting spinel and partially melted biotite using spinel rim and core compositions plot across the line of best fit for the experimental data for 850 °C. The core and rim compositions of spinel coexisting with new biotite suggest temperatures of between 780 and 825 °C. These results are clearly in reasonable agreement with Grapes' original temperature estimate and also suggest that the Mg-Fe exchange between spinel and biotite is not particularly sensitive to pressure. The problem with using Grapes' data is that the spinels have suffered some oxidation at the rims which may well affect the partition coefficient.

Estimates of reaction time

The experimentally-produced reaction microstructures reported in Brearley (1987) can be used

to place constraints on the possible times available for the transformation in the xenolith, although there are limitations. The most fundamental of these is the problem of comparing reaction microstructures obtained in isothermal experiments with those produced naturally under non-isothermal conditions. Clearly considerable caution must be exercised when carrying out such comparisons.

In addition, it is possible that some of the differences between the experimental and natural microstructures are attributable to the slower heating rates in the xenoliths in comparison with the experiments. Rapid heating rates will promote nucleation of the kinetically most favourable phase rather than the phase which should be stable on thermodynamic grounds as predicted by Ostwald's step rule (Putnis and McConnell, 1980). In the experimental work the development of melt rather than K-feldspar is attributable to behaviour of this type with melting taking place by metastable melting reactions (Brearley, 1987). These reactions are not predicted from the available experimental data on the equilibrium breakdown of biotite. The observation of melt in the natural example also implies that metastable melting has occurred and suggests that differences in heating rates (within certain limits) may not have an especially important effect. This conclusion is supported by preliminary experimental results on the effect of rates of heating on the reaction pathway using natural biotite (Brearley, unpublished data).

The experimental data for run durations up to 48 hours at 800 °C show that the extent of reaction is considerably greater than that observed in the natural biotite. The microstructure of a typical area

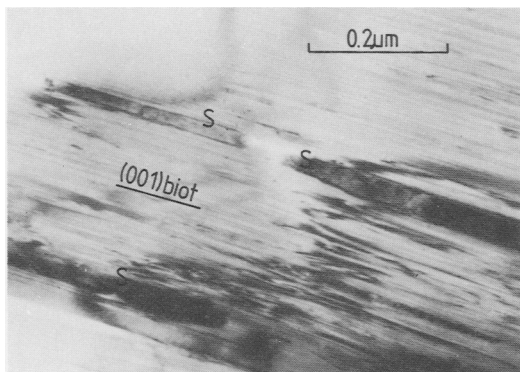


FIG. 11. Electron micrograph showing microstructure of biotite experimentally reacted at 800 °C, 1 kbar for 48 hours (QFM buffer). The development of spinel (S) is very significantly more widespread than in the naturally reacted biotite, cf. Fig. 3.

of biotite after the experiment is shown in Fig. 11. The development of spinel and melt is very much more widespread, but the spinels are significantly smaller than those in the natural example. Orthopyroxene, a phase not observed in this study, was identified locally in the experimental run products. After run times of greater than 48 hours, significant development of melt and orthopyroxene was observed.

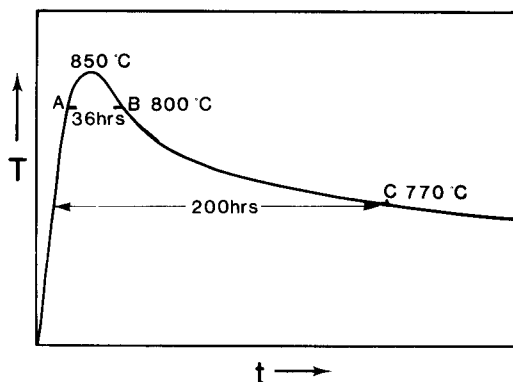


FIG. 12. Hypothetical temperature-time path followed by the xenolith. From a comparison of the experimental and natural reaction microstructures the maximum time spent above 800 °C (between A and B) must have been less than 48 hours. The total time above 770 °C can be estimated to have been less than ~200 hours from the analysed spread in spinel compositions coexisting with biotite. Between B and C nucleation ceases but the reaction continues until the closure temperature, C, is reached.

The differences between the experimental and natural reaction microstructures and reaction products must be interpreted in terms of the possible heating and cooling path followed by the xenolith. A hypothetical temperature-time ($T-t$) history is shown in Fig. 12 in which the heating stage was rapid and the maximum temperature was attained in a relatively short period of time. The most immediate and obvious conclusion which can be drawn from a comparison of the reaction microstructures is that, if the xenolith was above 800 °C for any period of time, it must have been for significantly less than 48 hours. Because of the exponential dependence of the nucleation rate on temperature, if a peak maximum temperature of, for example, 850 °C was reached, a very much higher density of spinels can reasonably be expected to have developed within the biotite. It seems probable, therefore, that the part of the temperature-time path (between A and B in Fig. 12)

spent above 800 °C, involving the period of rapid heating to the metamorphic maximum and subsequent cooling, lasted for perhaps 12–24 hours. During this period, nucleation of spinel will have commenced during the up-temperature part of the path and continued during the early part of the cooling history until the nucleation rate decreased to zero.

An additional constraint on the total time which the xenolith spent above 770 °C can be extracted from the experimental data. Analytical data for coexisting spinel and biotite obtained from several experimental runs of between 24 and 1600 hours (Brearley, 1987) show that the earliest spinels to nucleate are magnetite-rich, but become more hercynitic and Mg-rich as a function of time. This effect may be attributable to slow long-range diffusion of Mg and Al, in comparison with Fe, so that the compositions of the spinels are effectively controlled by kinetic factors, i.e. diffusion rates. The early spinels are thus metastable and change composition to that of the near-equilibrium or equilibrium composition.

During an experiment of, for example, 48 hours, nucleation of spinel will occur throughout the duration of the run. It can therefore be expected that, because of the diffusion control on the spinel chemistry, a whole range of spinel $\text{Mg}/(\text{Fe}^{2+} + \text{Fe}^{3+})$ values will be observed, depending on when they nucleated during the experiment. Spinel which nucleates early will have reacted to a composition which is closer to the equilibrium composition (i.e. will be more hercynitic) than spinel which nucleates towards the end of the experiment. Thus, as long as nucleation is occurring, the longer the experiment the larger the spread of spinel compositions. It is apparent that after extended runs the nucleation rate decreases as shown by the experimental data for a run of 1600 hours which contain no very magnetite-rich spinels. This suggests that, as the reaction proceeds, potential nucleation sites are consumed and thus the nucleation rate eventually reduces to zero. Once nucleation has ceased the spinel compositions will approach the equilibrium composition. The spread in the data for the $\text{Mg}/(\text{Fe}^{2+} + \text{Fe}^{3+})$ ratios of coexisting spinel and biotite can thus be used as a relatively sensitive indicator of the length of time for which the reaction proceeded.

To illustrate this point, contours are plotted in Fig. 13 to show the maximum and minimum $\text{Mg}/(\text{Fe}^{2+} + \text{Fe}^{3+})$ ratios obtained from coexisting spinel and biotite after run durations of 24, 48, 150, and 1600 hours. Convergence of all the contours will take place towards the equilibrium composition of coexisting biotite and spinel. It is uncertain whether equilibrium compositions have been ob-

tained in any of the experiments carried out to date so the convergence value is uncertain.

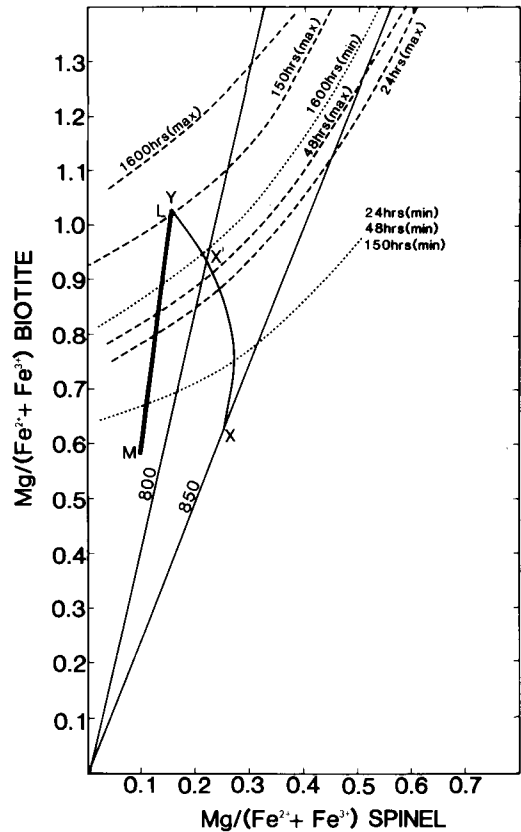


FIG. 13. Diagram showing the spread in $\text{Mg}/(\text{Fe}^{2+} + \text{Fe}^{3+})$ ratios of coexisting spinel and biotite as a function of experimental run time at 1 kbar. Lines of best fit from Fig. 10 are shown for 800 and 850 °C. Contour lines are constructed for runs of 24, 48, 150 and 1600 hours duration from Brearley (1987) to define the range of biotite and spinel $\text{Mg}/(\text{Fe}^{2+} + \text{Fe}^{3+})$ ratios observed in each run. These contour lines define the maximum and minimum $\text{Mg}/(\text{Fe}^{2+} + \text{Fe}^{3+})$ ratios observed in coexisting biotite and spinel and show that the range expands with increasing run time at each temperature up to run durations of 150 hours. Between 150 and 1600 hours nucleation ceases and the range of spinel compositions contracts, as exemplified by the maximum and minimum contour lines for 1600 hours. The contour for the maximum value of $\text{Mg}/(\text{Fe}^{2+} + \text{Fe}^{3+})$ for coexisting spinel and biotite after 1600 hours represents the hypothetical equilibrium mineral compositions. The line L-M represents the range of compositions found in coexisting spinel and biotite from this study. A hypothetical composition path (X-X¹-Y) followed by spinel and biotite from the xenolith is shown for a spinel which nucleates at point X at 850 °C.

These data can be used semi-quantitatively to constrain further the time available for the natural biotite to react, provided the effect of the non-isothermal behaviour of the xenolith is taken into consideration. The range of values observed in the xenolith is shown on Fig. 13. This comparison suggests that, had the natural biotite reacted in the xenolith isothermally, the spread in spinel compositions could have been achieved after about 200 hours (taking into account the initial differences in $\text{Mg}/(\text{Fe}^{2+} + \text{Fe}^{3+})$ between the biotites used for the experiments and those in this study). However, because of the non-isothermal path followed by the xenolith, the actual time taken is likely to have been somewhat shorter than this. Some spinels will clearly have nucleated and compositionally evolved at temperatures higher than 770 °C, so that for the early part of their history their compositions will change more rapidly. For example, a spinel nucleating at 850 °C at point X in Fig. 13 will follow a compositional path such as that shown to point Y at 770 °C. For the part of the path spent above 800 °C, between X and X¹, the composition of the spinels will change rapidly while the temperature is high. By the time the temperature has dropped to 800 °C, after perhaps 24 hours, the composition of the coexisting spinel and biotite will be closer to an equilibrium composition than would result from isothermal reaction for 24 hours at 800 °C. As cooling proceeds to 770 °C the change in composition of coexisting spinel and biotite will become progressively more sluggish as diffusion rates decrease. The temperature of 770 °C probably represents the closure temperature for diffusion between the two phases.

The most important conclusions to be drawn from these observations is that the amount of time taken by the xenolith to reach the closure temperature (770 °C) must have been less than 300 hours, perhaps about 200 hours. This time scale is consistent with estimates of cooling rates based on the heat flow data of Jaeger (1957). The broad spread in spinel compositions suggests that nucleation of new spinel probably occurred for a substantial part of this time. It is evident that, during the period of cooling, growth of spinels will continue and, although nucleation may have ceased, the reaction will still proceed. This is clearly the most important factor in producing larger spinels than those found in the biotites that were reacted experimentally at 800 °C and quenched before significant grain growth could occur.

Conclusions

TEM and AEM observations of stranded reaction microstructures show that the breakdown of

biotite under pyrometamorphic conditions takes place by the reaction:

$$\text{Fe-Al-biotite} = \text{Mg-Al-biotite} + \text{magnetite} + \text{hercynitic spinel} + \text{K-feldspar or melt} + \text{vapour}$$

as predicted by the experimental data of Eugster and Wones (1962) and Rutherford (1973). The reaction takes place by a topotactic mechanism with the orientations of the product phases controlled by the crystallography of the reacting biotite.

Using an empirical method based on the $\text{Mg}/(\text{Fe}^{2+} + \text{Fe}^{3+})$ ratios of coexisting spinel and biotite from experimental data, the reaction was deduced to have occurred above 770 °C. Temperatures of between 800 and 850 °C may have been attained for short periods of time at the peak of the temperature-time path. A comparison of the reaction microstructures with those obtained by experimental methods suggests that this must have been less than 48 hours.

From the experimental data on the change in spinel and biotite compositions as a function of time, it is evident that temperatures above 770 °C were likely to have been maintained for up to 200 hours, clearly showing that the drop in temperature during the early part of the reaction was extremely rapid. Brearley (1986) originally suggested that the maximum temperature reached by the xenolith may have been around 900 °C with the temperature falling to around 770 °C after about 4 days estimated from the data of Jaeger (1957). The experimental data presented here suggest that this estimate of the maximum temperature is too high, and that the overall time for cooling to 770 °C also took rather longer.

In conclusion, it is clear that TEM studies of naturally and experimentally reacted minerals within a rock matrix is a useful way of examining disequilibrium reaction mechanisms in metamorphic rocks. The comparison of experimentally-produced reaction microstructures with stranded microstructures in nature can provide data on rates of transformation and hence possible cooling times for small intrusions. However, in order to improve our understanding of these reaction mechanisms and to constrain further reaction times, the effects of non-isothermal *T-t* paths need to be investigated experimentally and combined with thermal modelling of intrusions. In addition, the effects of different rates of heating, pressure and the compositions and microstructures of the starting minerals need to be studied in detail.

Acknowledgements

The author wishes to thank D. C. Rubie, P. E. Champness, C. M. B. Henderson, G. T. R. Droop, R. H.

Jones and an anonymous reviewer for their constructive criticisms which have substantially improved the manuscript. D. A. Plant and T. C. Hopkins are thanked for their assistance with the electron microprobe analyses. Invaluable advice with the electron microscopy was given by Graham Cliff, Ian Brough and Pete Kenway of the Joint Manchester University/UMIST Department of Metallurgy. This work was carried out during an NERC Post-doctoral research fellowship which is gratefully acknowledged.

References

- Abraham, K. and Schreyer, W. (1973) *Contrib. Mineral. Petrol.* **40**, 275-92.
- Barber, D. J. (1970) *J. Mater. Sci.* **5**, 1-8.
- Brearley, A. J. (1984) Unpubl. PhD. thesis. Univ. of Manchester.
- (1986) *Mineral. Mag.* **50**, 385-97.
- (1987) *Bull. Mineral.* in press.
- and Champness, P. E. (1986) *Mineral. Mag.* **50**, 621-33.
- Cliff, G. A. and Lorimer, G. W. (1975) *J. Microsc.* **103**, 203-7.
- Eugster, H. P. and Wones, D. R. (1962) *J. Petrol.* **3**, 82-125.
- Grapes, R. H. (1986) *Ibid.* **27**, 343-96.
- Jaeger, J. C. (1957) *Am. J. Sci.* **255**, 306-18.
- Labotka, T. C. (1983) *Am. Mineral.* **68**, 900-14.
- Le Maitre, R. W. (1974) *J. Petrol.* **15**, 403-12.
- McGill, R. J. and Hubbard, F. H. (1981) In *Qualitative microanalysis with high spatial resolution* (Lorimer, G. W., Jacob, M. H., Doig, P., eds.) The Metals Society.
- Putnis, A. and McConnell, J. D. C. (1980) *Principles of mineral behaviour*. Blackwell Scientific Publications.
- Rubie, D. C. (1986) *Mineral. Mag.* **50**, 399-415.
- and Brearley, A. J. (1986) *Geol. Soc. Newsletter* **15**, no. 2, 46-7 (abs).
- (1987) *Bull. Mineral.* in press.
- Rutherford, M. J. (1973) *J. Petrol.* **14**, 159-80.
- Spear, F. S., Rumble III, D. and Ferry, J. M. (1982) *Reviews in Mineralogy*. **10**, 53-104. Min. Soc. Am.
- Smith, D. G. W. (1965) *Am. Mineral.* **50**, 1982-2022.
- Stewart, F. H. (1942) *Mineral. Mag.* **26**, 260-6.
- Wones, D. R. and Eugster, H. P. (1965) *Am. Mineral.* **50**, 1228-72.
- Burns, R. G. and Carroll, B. M. (1971) *Trans. Am. Geophys. Un.* **52**, 369.
- Worden, R., Champness, P. E., and Droop, G. T. R. (1987) *Min. Mag.* **51**, 107-21.

[Revised manuscript received 1 September 1986]